Pergamon

*Int. J. Heat Mass Transfer.* Vol. 41, Nos 4–5, pp. 671–680, 1998

Printed in Great Britain
0017-9310/98 $19.00+0.00

PII: S0017-9310(97)00243-3

# Numerical study of heat transfer from an impinging jet

PETER R. VOKE
Department of Mechanical Engineering, The University of Surrey, Guildford GU2 5XH, U.K.

and

SHIAN GAO
Department of Engineering, University of Leicester, Leicester, U.K.

(*Received* 5 *March* 1997 *and in final form* 18 *September* 1997)

**Abstract**—A computational study of the impingement of a thermally inhomogeneous turbulent jet on a solid plate, using large-eddy simulation, is reported. We investigate the case of a plane jet of water issuing from a plane channel into an enclosed pool and impinging normally on a perspex plate 1.8 jet-widths downstream. It is shown that the dynamics of the turbulence in this particular geometry results in the temperature variations at the plate surface having very high lateral correlation, so that lateral conduction of heat within the plate fails to have any significant effect on the transmission of thermal fluctuations from the fluid into the plate. By this means a simple one-dimensional model of the thermal, interaction between the media may be justified. © 1997 Published by Elsevier Science Ltd.

## 1. INTRODUCTION

Problems connected with the interaction of heated turbulent fluid and supporting structures are well known. Since the temperature of the fluid varies, turbulence in the fluid results in turbulent temperature fluctuations being transmitted into the solid structures, producing varying thermal stresses [1]. To obtain knowledge of such stresses it is first necessary to predict the thermal fluctuations in the turbulent fluid and then the manner in which they are modified by and pass into the solid boundaries. Important aspects of engineering design may depend not merely on mean temperatures or predictions of temperature variances, but on relatively rare peak levels and extrema [2]. For this reason, there are limits to the extent that traditional closure methods for the prediction of the flows are useful.

In large-eddy simulation (LES), turbulent flow is predicted by integrating the three-dimensional time-dependent Navier–Stokes equations directly, rather than through the use of a Reynolds-average model. The simulation must be performed in such a way that the solution becomes unstable in the same manner as the real physical fluid. A simulation in which all the physical scales of motion are completely resolved is called a direct numerical simulation. DNS is prohibitively expensive at high Reynolds numbers and can only be carried out for very low turbulent Reynolds numbers in which the range of scales present is severely restricted, while a large-eddy simulation, which is a numerical simulation in which not all the physical motions are resolved, can be performed for realistic engineering flows at high Reynolds numbers.

Those motions which cannot be resolved on the mesh in an LES are referred to as subgrid scale. These motions have a very important role in interchanging energy with the large resolved eddies, and so cannot simply be neglected: their effects are represented by a subgrid-scale model. A relatively simple eddy-viscosity model will often suffice to represent the action of the subgrid scales in an LES, based on the grid size as a length scale and the strain rate to define a velocity scale. This produces a model which is guaranteed to remove energy from the resolved scales.

A large-eddy simulation can give a much more realistic picture of certain aspects of turbulence than a closure model in many cases. In particular, it can display instantaneous fluctuations, turbulent flow structures, time traces of quantities, spectra and two-point correlations.

Large-eddy simulation has been used for the study of problems related to heat transfer in nuclear plant since the pioneering work of Schumann [3]. Round jets have been studied by Direct Numerical Simulation by Verzicco and Orlandi [4], Brancher *et al.* [5] and Boersma *et al.* [6]. Coannular jet flows have been simulated by LES by Akselvoll and Moin [7], Abba *et al.* [8] and Olsson and Fuchs [9]; the thesis by Olsson [10] contains a review of recent LES work on circular jets. More complex jet flows that have been studied include the LES of a plane jet in cross-flow by Jones and Wille [11] and the LES of a circular impinging jet by Olsson and Fuchs [12]. Mixing has

## NOMENCLATURE

| | |
|---|---|
| $A^+$ | wall layer scale constant |
| $c_S$ | Smagorinsky constant |
| $c_1$, $c_2$ | constants for split subgrid-scale model |
| $h$ | half-width of channel |
| $k_z$ | wavenumber for the $z$ direction |
| $\ell'$ | distance to nearest solid surface |
| $Pe_{mean}$ | mean flow Peclet number |
| $Re_{mean}$ | mean flow Reynolds number |
| $s$ | scalar magnitude of strain rate tensor |
| $\bar{s}$ | scalar magnitude of mean strain rate |
| $\tilde{s}$ | scalar magnitude of fluctuating strain rate |
| $s_{ij}$ | fluid rate of strain tensor |
| $\bar{s}_{ij}$ | mean fluid rate of strain tensor |
| $\tilde{s}_{ij}$ | fluctuating rate of strain tensor |
| $T$ | temperature (K) |
| $T'$ | root-mean-square temperature fluctuation (K) |
| $U$ | mean flow velocity at jet efflux plane |
| $u_\tau$ | mean friction velocity in channel |
| $u'$ | root-mean-square streamwise velocity fluctuation |
| $\overline{u'v'}$ | principal Reynolds stress |
| $v'$ | root-mean-square lateral velocity fluctuation |
| $x$ | streamwise coordinate |
| $y$ | lateral coordinate |
| $z$ | spanwise coordinate. |

Greek symbols

| | |
|---|---|
| $\Delta$ | measure of the grid size |
| $\Delta x$ | $x$ grid spacing (local) |
| $\Delta y$ | $y$ grid spacing |
| $\Delta z$ | $z$ grid spacing |
| $\nu$ | molecular kinematic viscosity |
| $\nu_{sg}$ | subgrid-scale eddy viscosity |
| $\nu_1$, $\nu_2$ | subgrid-scale eddy viscosities for split model. |

been studied recently in LES by Meinke *et al.* [13]. The present work is an LES study of a plane impinging jet, building on the preceding LES by Tsai *et al.* [14].

The principal objectives of the present work are:

- to reproduce the turbulent dynamics of a plane jet of water impinging on a normal surface of perspex;
- to predict the ratio of peak-to-peak temperature fluctuation to r.m.s. temperature fluctuation (a ratio known as the crest factor);
- to understand the effects of the solid surface on the turbulence and on the heat transfer from fluid to solid;
- to encapsulate the understanding of the dynamics of the heat transfer in a simple model.

Selected results from experiments very similar to the simulation reported here, and related closure computations, have been published by Morss [2]. Water and perspex were chosen deliberately by Morss in order to approximate the relative conductivities of liquid sodium impinging on steel, thus increasing understanding of thermal stressing in fast reactors. In the experiments a thermally inhomogeneous circular jet of water emerged into a wider cylinder and then impinged onto a solid perspex plate; the geometry is shown in Fig. 1(a). The geometry of our simulation, Fig. 1(b) is very similar, except that the symmetry is not cylindrical since the jet is planar rather than circular, and the outflow is sideways rather than normal to the impingement surface.

Previous simulation studies [14], on which we build, tested concepts allowing the simulation of spatially developing flows and their application to the thermal stressing problem.

## 2. METHODS

A finite-volume LES code was used for this study, designed for simulating three-dimensional time-dependent turbulent flows having one homogeneous dimension. It uses the Arakawa scheme [15] which conserves momentum, mass, and advected kinetic energy to machine accuracy, while computing the momentum fluxes across cell boundaries and the volume mean pressures approximately to second order in the mesh size. A similar code was used to perform channel flow simulations which provided inflow boundary data for the simulation of the jet. Both codes integrate the Navier–Stokes equations forward in time using the Adams–Bashforth scheme. The time step $\Delta t$ was kept well within the CFL and viscous limits, giving good temporal resolution of the fluctuating flow field.

The temperature was computed as a passive field obeying enthalpy convection equations: the discretisation was similar to that for the momentum equations except that second-order flux-limited upwind interpolation was used to avoid overshoot which can otherwise lead to violation of second-law constraints. The numerical diffusion that results is unavoidable but was estimated to be no larger than 25% of the total diffusion effects from molecular and eddy viscosity, at worst. No buoyancy effects were included since these were of no interest in this study,

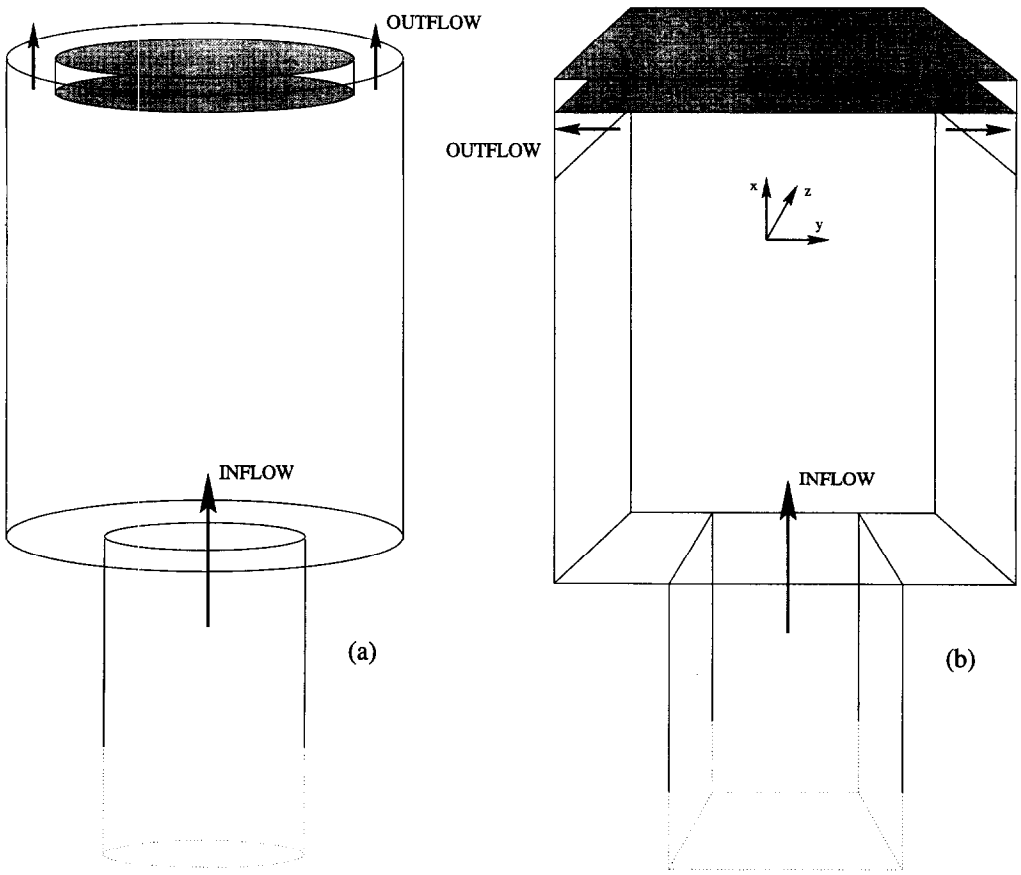


Fig. 1. Geometry of (a) the impinging jet experiment [2] and (b) the simulation.

so the thermal and momentum fields were dynamically decoupled.

The pressure field, which must be solved implicitly, was computed by use of the continuity equation, which gives rise to a Poisson equation by a familiar route. The periodicity of the solution in one dimension (in our case the $z$ coordinate) was utilised to Fourier transform in $z$, giving a sequence of Helmholz problems, one for each wavenumber $k_z$. These equations are solved by a vectorised cyclic reduction method, following Schwartztrauber [16] and Gavrilakis [17]. For the channel simulations, two dimensions are Fourier transformed, leading to an even simpler algorithm for the pressure solution. Further details of the numerical methods employed are given in Voke *et al.* [18].

The subgrid-scale model used was based on the original model of Smagorinsky [19], in which a subgrid eddy viscosity is derived from the local grid scale $\Delta$ and strain rate $s$:

$$\nu_{sg} = (c_S \Delta)^2 s \tag{1}$$

where

$$s^2 = 2 s_{ij} s_{ij} \tag{2}$$

and the constant $c_S$ is known as Smagorinsky's constant. The local grid scale is defined as

$$\Delta = (\Delta x \, \Delta y \, \Delta z)^{1/3}. \tag{3}$$

For an LES of homogeneous isotropic turbulence with the grid scale lying in the inertial subrange, the value of the Smagorinsky constant should be 0.23. The model is unsuitable for a wall-bounded flow, where the subgrid eddy viscosity must become zero at the wall. A number of workers have suggested modifications to the model for wall-bounded and free shear flows. Schumann [3] proposed that the interaction of the SGS with the mean strain $\bar{s}_{ij}$ should be modelled separately from its interaction with the resolved fluctuating strain; this gives rise to two separate subgrid eddy viscosities

$$\nu_1 = (c_1 \Delta)^2 \bar{s} \tag{4}$$

$$\nu_2 = (c_2 \Delta)^2 \tilde{s} \tag{5}$$

defined in terms of the span-average strain $\bar{s}^2 = 2\bar{s}_{ij}\bar{s}_{ij}$ and the span-fluctuating strain $\tilde{s}^2 = 2\tilde{s}_{ij}\tilde{s}_{ij}$, where the fluctuating strain rate $\tilde{s}_{ij}$ is the difference between the local instantaneous strain rate $s_{ij}$ and the strain rate

averaged over the spanwise dimension, $\bar{s}_{ij}$. The subgrid stress which enters the equations is then

$$\nu_1 \bar{s}_{ij} + \nu_2 \tilde{s}_{ij}. \tag{6}$$

$c_1$ is often lower than $c_2$, and both are found to take lower values in wall-bounded flows than in free shear flows. If $\nu_1$ is set to zero, the interaction of the SGS with the mean shear is eliminated entirely. The values used in our simulations were $c_2 = 0.1$, $c_1 = 0$ for the channel and $c_2 = 0.23$, $c_1 = 0$ for the jet. (These constants were given incorrectly in [18].)

The subgrid eddy viscosity must vanish at solid surfaces, a requirement achieved by modifying the length scale $\Delta$ with a damping factor of the form

$$\Delta \leftarrow \Delta[1 - \exp(-\ell^+/A^+)] \tag{7}$$

where $\ell$ is the perpendicular distance from the point in question to the nearest solid surface. Near an internal or external corner the definition of $\ell$ is generalised to

$$\frac{1}{\ell} = \oint \frac{\mathrm{d}\theta}{2r(\theta)} \tag{8}$$

where $r(\theta)$ is the radial distance of each part of the wall from the point in question. (The definition of $\ell$ was also given incorrectly in [18].) $A^+$ was equal to 25 in our simulations.

A subgrid diffusion also acts on the temperature field, since enthalpy is transported by the unresolved eddies. The usual approach is to employ a subgrid eddy Prandtl number, which embodies the assumption that the transport of enthalpy is closely related to the transport of momentum. The value used in our simulation was 0.3, based on the study of Antonopoulos-Domis [20].

## 3. THE SIMULATION

The half-width of the channel $h$ was taken as unit width, equivalent to 36 mm in the impinging jet experiment [2]. The width of our pool was $4.25h$ and the width of the plate was $3.5h$; both dimensions were very close to the experiment. The impingement plate was $3.61h$ from the plane of the jet, just as in several of the runs in the experiment [2]. This simulation is Case 4 of [18].

Velocities are given in non-dimensional units based on the nominal shear velocity $u_\tau$ on the walls of the channel. This means that the unit of time, $h/u_\tau$, which on dimensional grounds is the time-scale of the large eddies in the upstream channel flow, was equivalent to 6.74 s in the experiment [2], where $u_\tau$ was 5.34 mm/s. The temperatures are given between 0 and 15, equivalent to the range of 15 K in the impinging jet experiment of Morss [2].

To achieve adequate resolution in the $x$ direction, the $x$ mesh was compressed from the upstream end of the jet simulation, where the spacing matched that used in the channel simulation at $\Delta x = 0.1963h$ at the plane of the jet, to $\Delta x = 0.0028h$ at the impingement plate. The total number of $x$ meshes used in the fluid was 63. This resulted in a mesh that was easily fine enough for the application of natural no-slip boundary conditions at the plate; based on the largest shear on the plate, the point nearest the plate was at $x^+ = 0.4$. The $y$ mesh was uniform, with 32 meshes across the channel and 68 across the pool, giving $\Delta y = 0.0625h$. The $z$ mesh was also uniform, with 64 mesh cells across the width of $\pi h$, so that $\Delta z = 0.0491h$. Our methods use a staggered mesh arrangement.

We also studied the thermal field in the solid plate on which the flow impinged, and the correlations between the temperature fluctuations in the plate and in the fluid. An additional nine $x$ mesh cells were set up inside the plate, with one point very close to the surface ($\Delta x = 0.0014$) and stretched in the plate ($\Delta x = 0.1913$ at the back of the plate).

In order to simulate the complete jet geometry, we ran two simulations in conjunction, one to predict the channel upstream of the jet efflux plane, and the other to predict the jet itself, the pool into which it issued, and also the plate on which it impinged. The two simulations were designed to ensure that the meshing in all three dimensions and the time step were matched, and that boundary conditions and fluid properties were compatible. The channel flow simulation was run first, and velocity and temperature data on a plane perpendicular to the flow direction at the downstream end of the channel were recorded on disc at every time step. These data were used to define the inflow velocity components and temperature for the jet simulation subsequently.

The solid-wall boundary conditions used in the channel and jet simulations vary according to the flow conditions. In the channel, the mean wall shear and resolution are such that the first mesh point adjacent to the wall is not close enough to apply no-slip conditions, nor so far away that a log-law artificial boundary condition is always appropriate. The instantaneous flow field was monitored and an appropriate artificial boundary condition based on the log-law, the non-slip condition, or the Von Kármán interpolation is imposed, as described by Voke *et al.* [18].

For the jet, the inflow region was $2h$ wide. On the inflow plane, velocities obtained from the channel simulation were utilised at each time step as a boundary condition on the jet velocity. The outflow regions on either side of the impingement plate were $0.75h$ wide. On these planes a convective condition [21] was used to fix an outflow velocity component.

The thermal boundary conditions in the channel simulations were chosen to produce a good match to the experimental temperature profiles at the jet efflux plane. At the upstream end of the channel the temperature had a discontinuous profile across the channel, with a central plateau of width $1.06h$ at $T = 15$ between two regions of width $0.47h$ at $T = 0$. The temperature profile and fluctuation levels then

developed naturally down the channel length, without any further heat transfer, since the channel walls were adiabatic. At the downstream end of the channel the thermal field was convected out of the end of the computational box using a convective boundary condition on the boundary plane. Temperature data were stored with the velocities and transferred to the jet simulation as thermal inflow conditions for the jet simulation.

The walls of the pool were adiabatic so that the transport of enthalpy occurs solely through inflow, outflow, and conduction into the impingement plate. The outflow thermal boundary conditions were convective, with the convecting velocity being the same as that used for the velocities. The velocity boundary conditions on the solid surfaces were treated in the same way as for the channel, though it was found that in all cases no-slip conditions were being applied; on the side walls where the mesh was quite coarse the velocities were low, while the $x$ mesh at the impingement plate was very fine.

The heat transfer from the fluid into the solid plate was the main focus of interest in this study. The interface was at the boundary of a temperature cell, across which a conductive heat flux was defined. The heat conducted out of the fluid was set equal to the heat conducted into the solid, and the conductive heat flux across the boundary and the temperature at the wall were computed from the temperatures at the last point in the fluid and at the first point in the solid, allowing for any difference in the thermal diffusivities of the two media. The conditions obtaining in the simulation are such that this conductive boundary condition is appropriate, rather than an artificial temperature boundary condition involving a wall model. The back surface of the plate was isothermal, with the temperature constant and equal to the time-mean temperature of the fluid flowing out of the jet simulation.

## 4. RESULTS

A large number of test runs was performed to check the reliability of the code and the innovations introduced, including laminar runs and runs with different Prandtl numbers and geometries.

The initial state in the jet simulation was very simple: the velocity and temperature fields were both zero, being built up entirely by flow into the computational volume through the inflow plane. The temperature field in the plate was set to a uniform gradient between the front and back boundary conditions, once the fluid had settled down to allow these temperature boundary conditions to be reliably estimated. Temperature fluctuations were then allowed to propagate into the solid. The simulation was conditioned over $10h/u_\tau$ before test simulations in various geometries were started, each run using the final condition of the previous run as its starting field.

The fluid Prandtl number was set to 6.95, the value appropriate for water, and the thermal diffusivity of the solid plate to 0.19 mm$^2$/s, a typical value for perspex. Governing parameters for the flow were $Re_{\text{mean}} = hU/\nu = 6500$, $Pe_{\text{mean}} = 45{,}175$.

The conditioning, test, and production simulations were all performed on Cray X-MP and Y-MP computers using a single processor. With $\Delta t$ set to $0.0002h/u_\tau$, each time unit of simulation $h/u_\tau$ took 5000 time steps. The total time covered by the simulation was $14h/u_\tau$, equivalent to about 94 s in the experiment [2]. This run required 52 cpu hours. The time step size was determined by the CFL limit, the highest value being 0.25. The maximum viscous number was about 0.03.

Figure 2 shows the profile of the time-average streamwise velocity $\bar{u}$ in the channel and the root-mean-square fluctuation $u'$ compared with the data of Nishino and Kasagi [22], normalised to the same peak velocity. The mean flow Reynolds number of the simulation (6500) is close to that of the experiment [22] (6560). The comparison indicates that the channel simulation is satisfactory; other statistics from the channel simulation were also satisfactory.

Figure 3 shows contours of the time-average streamwise velocity $\bar{u}$ in the jet simulation. The contours are very similar in shape to those of Morss [2], and confirm that the jet simulation is broadly reproducing the behaviour of a physical jet. Figure 4 shows a vector plot of the time-average velocity field in the jet. This clarifies the position of the double recirculation regions, and the direction of the flow over and round the plate. It is clear that the fluid in contact with the plate comes predominantly from the centre of the jet, though this observation can be modified by fluctuations. Both recirculation regions are double.

Figure 5 shows contours of the root-mean-square streamwise velocity fluctuation $u'$. The fluctuations emerging from the channel are reduced in the jet efflux region, but new ridges of fluctuation are clearly generated in the region of the jet boundaries, suggesting the existence of instabilities there producing turbulent fluctuations. Figure 6 shows contours of $v'$, the r.m.s. cross-stream fluctuation, which demonstrates clearly that there is production of turbulent fluctuations around the edges of the recirculation zones. Contours of the principal resolved Reynolds stress $\overline{u'v'}$ (not shown) confirm that the jet edges have become unstable and are generating new turbulence. These observations have also been clarified by video imaging of the jet and its impingement [23].

Figure 7 shows the contours of the mean temperature $T$ in the jet. The agreement with closure calculations reported by Morss [2] is satisfactory. Figure 8 shows contours of the r.m.s. temperature fluctuation $T'$: there is some deviation from the results produced by the corresponding experiment [2] in a cylindrical geometry, but comparison with the closure computations confirms that this is purely a geometric effect arising from the cylindrical symmetry of the experiment compared with the planar geometry of our simulation.

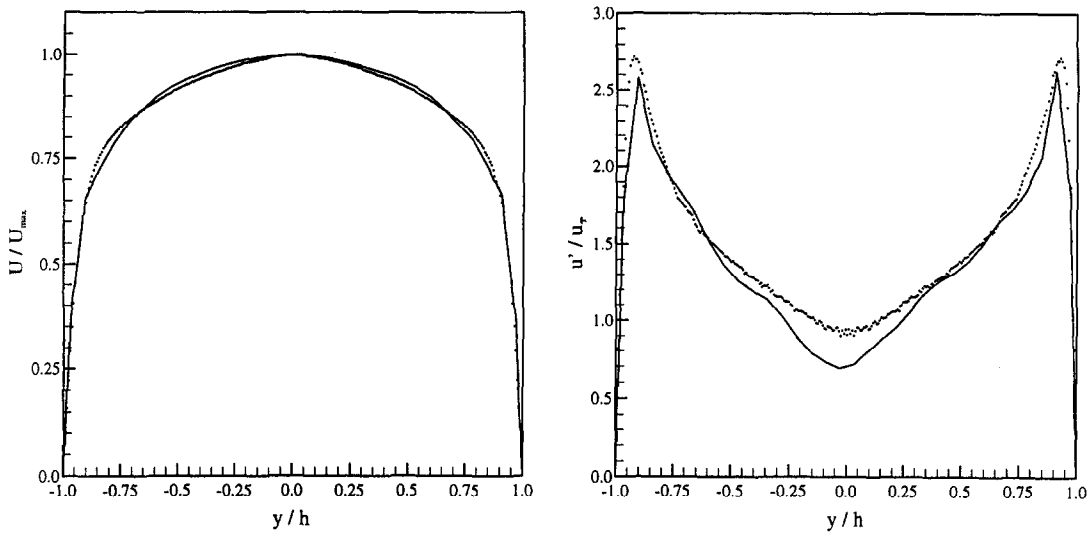


Fig. 2. Profiles of (left) streamwise velocity profile $\bar{u}$ in the channel and (right) r.m.s. streamwise fluctuation $u'$, lines; points, data of Nishino and Kasagi [22].

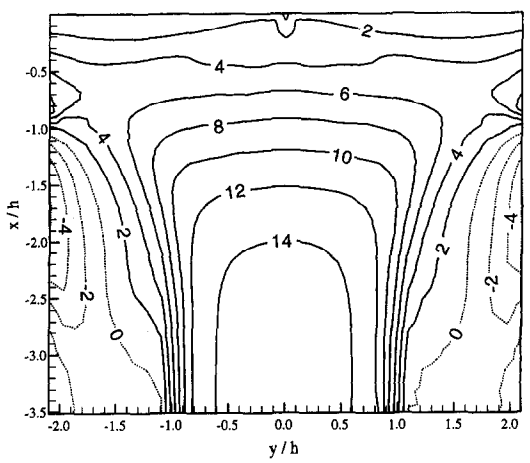


Fig. 3. Streamwise velocity contours $\bar{u}/u_\tau$ in the jet.

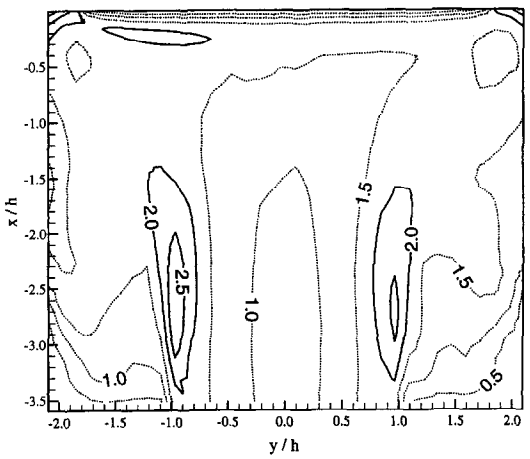


Fig. 5. Contours of streamwise r.m.s. turbulence fluctuation $u'$ in the jet.

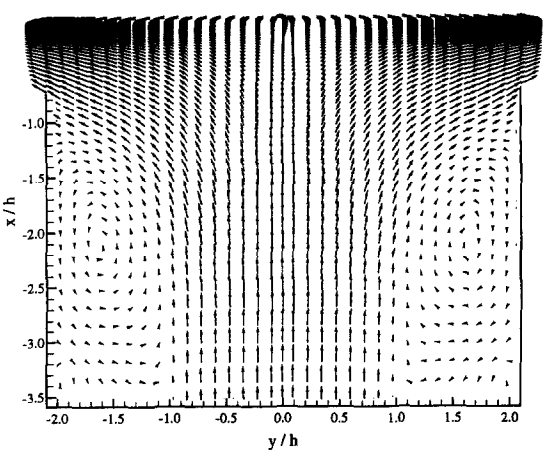


Fig. 4. Vectors of mean velocity $(\bar{u}, \bar{v})$ in the jet.

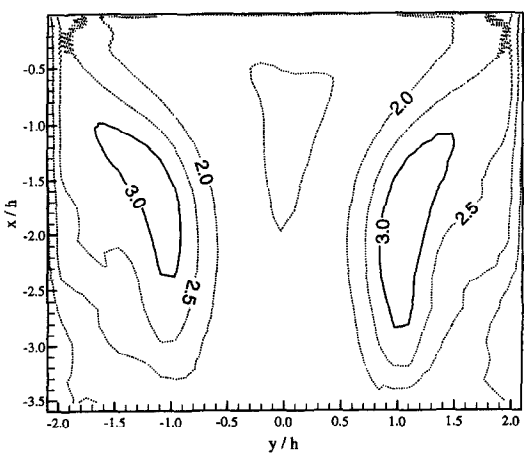


Fig. 6. Contours of cross-stream r.m.s. turbulence fluctuation $v'$ in the jet.

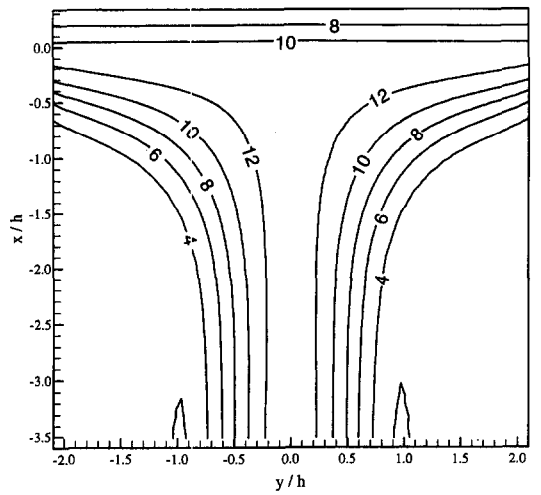


Fig. 7. Contours of mean temperature $\bar{T}$ in the jet and the solid plate: contour intervals in degrees. The total temperature difference set upstream in the jet was 0 to 15 degrees.

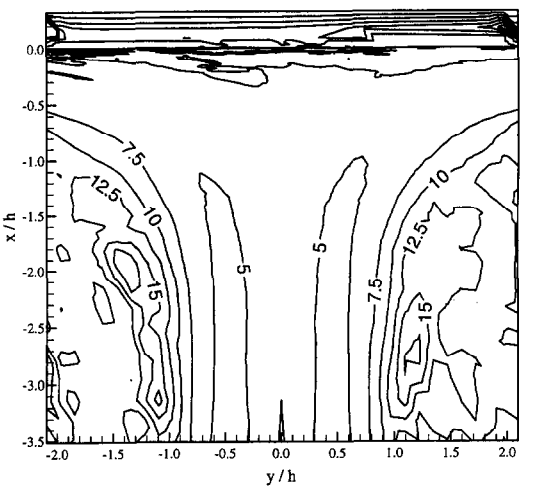


Fig. 9. Contours of temperature crest factor in the jet and in the plate.

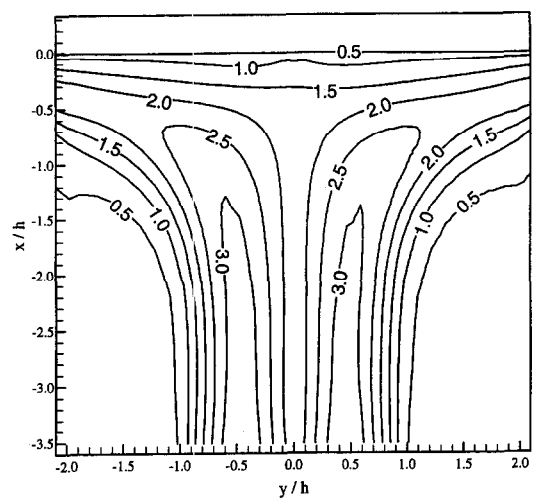


Fig. 8. Contours of temperature fluctuation $T'$ in the jet and in the plate, in degrees.

The behaviour of the extreme temperature variations was one of the principal matters of interest in this study. The extrema are quantified by means of temperature distributions gathered over the full $x$–$y$ plane of the jet. These allowed the extraction of various statistics, in particular $x$–$y$ distributions of peak-to-peak temperature swing, maximum and minimum temperatures, and the "crest factor". The crest factor is defined as the ratio between the peak-to-peak swing (the difference between the maximum and minimum temperatures encountered during the simulation at each point, also referred to by mathematicians as the $L_\infty$ norm) and the r.m.s. temperature fluctuation level (the $L_2$ norm).

The temperature crest factor $\Delta T/T'$ is shown in Fig. 9. This quantity appears to require a longer period of averaging to produce good quality statistics, but in fact it will always pick up the tails of the distribution of the temperature because of the way it is defined, and appear ragged. It is nevertheless possible to judge its distribution from the results shown. The regions of highest crest factor, which are found at the edges of the recirculation zones, reach a level of over 15. Only in the central part of the jet is the crest factor at or below 5. The large crest factors are found to be the result of low values of r.m.s. fluctuation rather than high peak-to-peak swing. The high level of crest factor occurring at the edges of the recirculation zones is due to very occasional excursions of warm fluid into the predominantly cold zones. These affect the peak-to-peak swing, but have relatively little effect on the r.m.s. value because of their rarity.

The behaviour of the crest factor up to the plate is clarified by studying the variation of the maximal and minimal temperatures encountered during the run. The maxima are consistently high right up to and into the plate, while the minimum values show greater variation as the plate is approached. It appears that the plate surface is protected by a layer of hot fluid which the cold incursions cannot displace. As a result, the minimum temperatures rise while the r.m.s. fluctuations reduce in the solid. The crest factor rises, since successful incursions of cold fluid into the inner layer close to the plate are rare, and prolonged incursions that can significantly lower the temperature inside the plate are even more rare. The crest factor drops off rapidly and smoothly inside the plate, and uniformly across the width, to reach a negligible level at the back of the plate. The maximum and minimum temperatures rapidly converge to nearly the same values inside the plate, explaining the rapid drop in peak-to-peak swing and crest factor within the perspex.

In addition the simulation has provided rich stat-

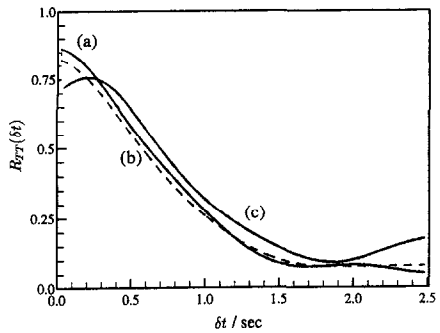


Fig. 10. Normalised lateral temperature two-point correlations in the fluid, close to the solid surface ($x = -0.014h$); (a) between centreline point $y = 0$ and point at $y = 0.805h$; (b) between $y = 0$ and $y = 1.195h$; (c) between $y = 0$ and $y = 1.61h$.

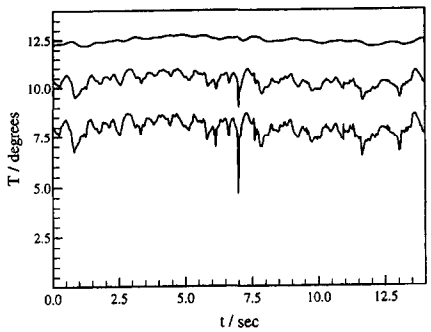


Fig. 11. Time histories of temperatures and the centreline $y = 0$ just outside and inside the solid. Lower curve, $x = -0.0014h$ (in the fluid); centre curve, $x = 0.0007h$ (plate surface); upper curve, $x = 0.026h$ (deeper in the plate). The lower two curves have been displaced vertically by 2.5 and 5 degrees respectively for clarity.

istics of the temperature within the solid plate. The main results are extracted from detailed time-traces or histories of temperature gathered at selected points in the water and in the perspex. Time traces were recorded of temperature, velocity components and pressure at 49 points in the fluid (negative $x$) and of temperature at 14 points in the solid (positive $x$). These reveal strong lateral correlations in temperature close to the plate, in agreement with the findings of Morss [2]. Points separated in $x$ only (streamwise separation) in the fluid are less well correlated.

Temperature autocorrelations, velocity autocorrelations and spectra have been computed at some of the points but are of limited relevance here and are omitted. The most instructive of the temperature two-point correlations are shown in Fig. 10: these are correlations between a point just outside the plate on the centreline and points separated laterally (in $y$). It is clear that a high temperature correlation persists across the plate laterally, as found experimentally [2]. The highest correlation for the points having the smaller $y$ separation occurs with zero time delay. Points separated in $x$ are found to have a much lower level of temperature correlation.

Temperature two-point correlations with points inside the plate (not shown) indicate that the temperature inside the solid may be governed by the integrated effect of the external temperature over some period, and also that the temperature inside the solid may be predicted on the basis of the temperature of the fluid in contact with it at the same lateral position. We should expect such behaviour if the diffusion timescale in the solid is shorter than the timescale of the thermal eddies in the impinging fluid. To test this hypothesis, a simple one-dimensional conduction model was constructed, with the temperature trace at the point $x = 0.0014h$, $y = 0$ as input. The model excluded all convection effects and the influence of temperature histories at points other than (0.0014, 0). It was used to predict the temperature histories at the surface and internal points (+0.0007, 0) and (+0.026, 0). Figure 11 shows the corresponding simulation temperature histories; on the scale of this graph the predictions of the one-dimensional model are indistinguishable from the actual temperature histories shown.

Table 1.

| | $x = 0.0007h$ | | $x = 0.026h$ | |
|---|---|---|---|---|
| | 3D | 1D | 3D | 1D |
| $T_{min}$ | 0.766 | 0.737 | 0.807 | 0.802 |
| $T_{max}$ | 0.896 | 0.903 | 0.850 | 0.844 |
| $T_{mean}$ | 0.860 | 0.855 | 0.829 | 0.823 |
| $T_{rms}$ | 0.023 | 0.026 | 0.0107 | 0.0107 |
| $T_{crest}$ | 5.57 | 6.38 | 4.00 | 3.94 |

We therefore conclude that the temperature at the surface of the plate drives that inside the plate by conduction and the mechanism is well modelled as a one-dimensional phenomenon. To quantify the similarity of the predictions of the one-dimensional (1D) model and the three-dimensional (3D) simulation, the maximum, minimum, mean, r.m.s. fluctuation and crest factor of the temperature are given in Table 1. Though the 1D model predicts the temperature variation a little high on the surface, it is clearly adequate for engineering purposes.

## 5. DISCUSSION

In order to understand the origin of the temperature fluctuations and their spatial distribution as revealed in the two-point correlations, continuous sequences of contours of the instantaneous temperature field in a single arbitrary $z$ plane have been studied by video imaging [23]. The mean temperature distribution in the jet serves to concentrate cold fluid predominantly near the boundaries and hot fluid in the centre, leading to a hot jet impinging on the plate and cold fluid in the recirculation regions. The instability of the jet

boundaries then causes entrainment of cold fluid into the central hot core of the jet, enhancing fluctuations already present in the jet efflux. Cold eddies form when fluid from the recirculation zones combines with the cold fluid at the edges of the jet and is entrained into the jet which then convects them towards the plate. It is apparent from the video sequences that the principal mechanism for the generation of large-scale temperature fluctuations is instability of the edge of the jet, causing entrainment of cold fluid from the recirculation zones.

The behaviour of the cold and hot eddies as they are carried onto the plate is also of great interest. Hot eddies are areas more or less elongated in the streamwise direction, identified by the presence of cold eddies at either end. These structures flatten in the $x$ direction and widen in the $y$ direction as they are carried towards the plate and since the convection velocity decreases the elongated hot and cold eddies linger in contact with the plate. Diffusion erodes the temperature differences throughout the process so that the eddies become less easy to identify unambiguously; nevertheless the origin of large lateral ($y$) two-point temperature correlations near and inside the plate is clear.

We find that the nearly stagnant hot fluid near the centre of the plate is at a mean temperature significantly higher than the mean temperature of the jet, and this layer of hot fluid in contact with the plate forms a buffer that makes it difficult for cold eddies to impinge directly onto the plate surface. The creation, by entrainment, of cold eddies which persist long enough to impinge directly onto the plate is relatively rare and significant lowering of the plate temperature by such an eddy is even more rare.

The distortion of the turbulence structures in the impingement region is found to lead to an increase in the $y$ integral correlation length for all variables, including the temperature, as the plate is approached. This is confirmed by computing two-point correlations both along and perpendicular to the plate. As a result, the temperature fluctuations in the plate are relatively independent of $y$.

These mechanisms produce lower temperature differences at the plate than is assumed by current engineering design methods. The normal assumption, that the mean temperature difference present at the plane of the jet may be transmitted into the plate, is clearly very pessimistic. The simulation reveals that the temperature swing in the thermal eddies that are convected towards the plate is related to the temperature of the recirculation zones, which consists of fluid already subjected to some thermal mixing. Also important is the strong attenuation of the thermal eddies as they move towards the plate and the protection of the plate by a layer of hot fluid. Our identification of these mechanisms suggests that forced mixing of the cool fluid in the recirculation zones with hot fluid may be a practical way of further reducing the magnitude of large thermal fluctuations and thermal stressing.

Thermal stressing is further reduced by the change in the structure of the eddies as they move towards the plate. They widen, leading to high lateral correlations in the temperature variation. The thermal stressing taking place in the geometry is primarily a temporal rather than a spatial phenomenon. It has low temporal frequency but is strongly correlated laterally across the plate. Thermal eddies at the centre of the jet are slowed in their convection as well as stretched and attenuated, remaining close to the plate for prolonged periods before being replaced by fluid of the opposite character, though in general the cold fluid seems to have difficulty in displacing the layer of hot fluid normally in contact with the plate. The widening of the eddies results in the solid also responding in a laterally correlated manner, with the temperature variations both at the surface and deeper in the perspex being closely related to the instantaneous temperature of the fluid in contact with the plate at the same lateral position. This finding has led us to propose that a simple one-dimensional conduction model for the response of the solid plate is adequate to describe its thermal behaviour.

*Acknowledgements*—This research was performed under cofunded grant GR/F 26089, supported by the Central Electricity Generating Board (later Nuclear Electric plc) and the U.K. Science and Engineering Research Council. We are particularly grateful to the technical correspondents at Berkeley Nuclear Laboratory, Drs Richard Szczepura, Tony Morss and Michael Reeks, for their support and their contribution to the success of this work. The computations were performed on Cray supercomputers at the Atlas Centre under grants of resources from the U.K. Science and Engineering Research Council, without which the research would not have been possible.

## REFERENCES

1. Ellison, E. G., Review of the interaction of creep and fatigue. *J. Mech. Eng. Sci.*, 1969, **11**, 318–339.
2. Morss, A., Impinging jet results at low Reynolds numbers for comparison with large eddy simulation calculations. *Nuclear Electric Memorandum TD/STB/MEM/0276*, Technology Division, Nuclear Electric, U.K. 1991.
3. Schumann, U., Subgrid scale model for finite difference simulations of turbulent flows in plane channels and annuli. *J. Comp. Phys.*, 1975, **18**, 376–401.
4. Verzicco, R. and Orlandi, P., Direct simulation of the transitional regime of a circular jet. *Phys. Fluids A*, 1994, **6**, 751–759.
5. Brancher, P., Chomaz, J. M. and Huerre, P., Direct numerical simulations of round jets: vortex induction and side jets. *Phys. Fluids*, 1994, **6**, 751–750.
6. Boersma, B. J., Brethouwer, G. and Nieuwstadt, F. T. M., Direct numerical simulation of a round turbulent jet. *DNS and LES of Complex Flows*, ed. Geurts and Kuerten. Mem. no. 1394, Univ. Twente, Netherlands, 1997, pp. 106–111.
7. Akselvoll, K. and Moin, P., Large eddy simulation of turbulent confined coannular jets. *J. Fluid Mech.*, 1996, **315**, 387–411.
8. Abbà, A., Bucci, R., Cercignani, C. and Vadettaro, L., LES simulation of turbulent coaxial jets using the

dynamic SGS model. *DNS and LES of Complex Flows*, ed. Geurts and Kuerten. Mem. no. 1394, Univ. Twente, Netherlands, 1997, pp. 88–93.
9. Olsson, M. and Fuchs, l., Simulation of a co-annular swirling jet using a dynamic sgs-model. AIAA paper 94-0654, 1994.
10. Olsson, M., Large eddy simulation of turbulent jets. Doctoral Thesis, Technical Report 1997 : 2, KTH Stockholm, 1997.
11. Jones, W. P. and Wille, M., Large-eddy simulation of a plane jet in a cross flow, *Int. J. Heat and Fluid Flow*, 1996, **17,** 296–306.
12. Olsson, M. and Fuchs, L., Large-eddy simulation of a circular impinging jet. Submitted for publication; included in [10], 1997.
13. Meinke, M., Schulz, C. and Rister, T., Large-eddy-simulations of the mixing processes in a spatially developing turbulent jet. *DNS and LES of Complex Flows*, ed. Geurts and Kuerten. Mem. no. 1394, Univ. Twente, Netherlands, 1997, pp. 100–105.
14. Tsai, H. M., Leslie, D. C. and Voke, P. R., Thermal striping : structures in interacting jets, in *Turbulence and Coherent Structures*, ed. Metais and Lesieur, Selected Papers from Turbulence '89. Kluwer Academic, 1991, pp. 125–138.
15. Arakawa, A., Computational design for long-term numerical integration of the equations of fluid motion : two-dimensional incompressible flow. Part 1. *J. Comp. Phys.*, 1966, **1,** 119–143.
16. Schwarztrauber, P. N., A direct method for the discrete solution of separable elliptic equations. *SIAM J. Num. Analysis*, 1974, **11,** 1136–1150.
17. Gavrilakis, S., Numerical simulation of low-Reynolds-number turbulent flow through a straight square duct. *J. Fluid Mech.*, 1991, **244,** 101–129.
18. Voke, P. R., Gao, S. and Leslie, D. C., Large-eddy simulations of plane impinging jets. *Int. J. Num. Methods of Engineering*, 1995, **38,** 489–507.
19. Smagorinsky, J., General circulation experiments with the primitive equations : part I, the basic experiment, *Monthly Weather Review*, 1963, **91,** 99–164.
20. Antonopoulos-Domis, M., Large-eddy simulation of a passive scalar in isotropic turbulence. *Int. J. Num. Methods Fluids*, 1981, **1,** 273.
21. Voke, P. R. and Potamitis, S. G., Numerical simulation of a low-Reynolds-number wake behind a flat plate. *Int. J. Num. Methods Fluids*, 1994, **19,** 377–393.
22. Nishino, K. and Kasagi, N., Turbulence statistics measurements in a two-dimensional channel flow using a three-dimensional particle tracking velocimeter. *Seventh Symposium Turbulent Shear Flows*, Stanford University, August 1989, Vol. 2, paper 22-1, 1989.
23. Gao, S. and Voke, P. R., Dynamics of thermal eddies in an impinging jet predicted by large-eddy simulation. *Visual. Engng. Res.*, 1996, **2**(1). See also http://vortex.mech.surrey.ac.uk/fluidata/.